

Frequency Dependent Specific Heat from Thermal Effusion in Spherical Geometry.

Bo Jakobsen, Niels Boye Olsen, and Tage Christensen*
*DNRF centre "Glass and Time," IMFUFA, Department of Sciences,
 Roskilde University, Postbox 260, DK-4000 Roskilde, Denmark*

(Dated: June 21, 2024)

We present a novel method of measuring the frequency dependent specific heat at the glass transition applied to 5-polyphenyl-4-ether. The method employs thermal waves effusing radially out from the surface of a spherical thermistor that acts as both a heat generator and thermometer. It is a merit of the method compared to planar effusion methods that the influence of the mechanical boundary is analytically known. This implies that it is the longitudinal rather than the isobaric specific heat that is measured. As another merit the thermal conductivity and specific heat can be found independently. The method has highest sensitivity at a frequency where the thermal diffusion length is comparable to the radius of the heat generator. This limits in practise the frequency range to 2–3 decades. An account of the 3ω -technique used including higher order terms in the temperature dependency of the thermistor and in the power generated is furthermore given.

PACS numbers: 64.70.P-

I. INTRODUCTION

A hallmark of the glass transition of supercooled liquids is the time dependence of physical properties — relaxation also called. This time dependence is typically seen on the timescale of the so-called Maxwell relaxation time τ_M . τ_M is defined as

$$\tau_M = \frac{\eta_0}{G_\infty} \quad (1)$$

where η_0 is the low frequency limiting shear viscosity and G_∞ the high frequency limiting shear modulus. The relaxation is often most easily studied in the frequency domain. At high frequency the liquid shows solid-like elastic behaviour whereas at low frequencies it shows liquid-like viscous behaviour. In general the viscoelastic stress response to oscillatory shear strain is jointly described by the complex dynamic shear modulus G [1]. The structural relaxation is also observed in the specific heat. This has long ago been studied in the time domain as enthalpy relaxation [2], but in 1985 frequency domain studies or AC-calorimetry [3, 4] were introduced in the research field of supercooled liquids. Common to these methods is that they excite thermal oscillations in the sample at a cyclic frequency ω . For a heat diffusivity, D , this frequency is associated with a characteristic heat diffusion length,

$$l_D = \sqrt{\frac{D}{i\omega}}, \quad (2)$$

the magnitude of which gives the range of the excited thermal waves. When comparing $|l_D|$ to a given sample size L one can classify AC-calorimetry experiments as to whether the sample is thermally thin ($L \ll |l_D|$) or thermally thick ($L \gg |l_D|$). A typical value of D is $0.1 \text{ mm}^2/\text{s}$ giving $|l_D| \approx 0.1 \text{ mm}$ for a frequency of $\nu = \omega/(2\pi) = 1 \text{ Hz}$. This means that thermally thin methods are confined to rather low frequencies [4] or very thin samples [5]. In these methods the temperature field is homogeneous throughout the sample and the frequency dependent specific heat is derived directly. The AC-technique allows for easy corrections of the influence of heat leaks in a non-adiabatic configuration. AC-calorimetry on thermally thick samples on the other hand has the advantage of covering a large frequency span [3, 6]. In this case the temperature field is inhomogeneous and what is really measured is the effusivity, from which the specific heat is derived. The effusivity $e = \sqrt{\lambda c}$ expresses the ability of the liquid to take up heat from parts of its surface and transport it away (thermal effusion). This ability is dependent on two constitutive properties, the heat conductivity λ and the specific heat (pr. volume) c . The specific heat can only be found to within a proportionality constant in effusion experiments from an (infinite) plane. However taking boundary effects into account for finite size plane heaters [7, 8] one may in principle find λ and c independently. The intermediate situation where the heat diffusion length is comparable to the sample thickness has been exploited in the so-called two-channel ac calorimeter [9, 10]. This fine method aims directly at an independent determination of λ and c .

The specific heat entering the effusivity is widely taken as the isobaric specific heat c_p . However recently it has been shown [11, 12, 13] that in planar and spherical geometries it is rather the longitudinal specific heat c_l that enters.

When M_S and M_T are the adiabatic and isothermal longitudinal moduli respectively, c_l is related to the isochoric specific heat, c_v by

$$c_l = \frac{M_S}{M_T} c_v. \quad (3)$$

In contrast, when K_S and K_T are the adiabatic bulk moduli respectively, c_p is given by

$$c_p = \frac{K_S}{K_T} c_v. \quad (4)$$

Now $M_S = K_S + 4/3 G$, and $M_T = K_T + 4/3 G$. This means that c_l will differ from c_p exactly in the relaxation regime where G dynamically is different from zero.

In this work we study the frequency dependent specific heat from thermal effusion in a spherical geometry. The justification is threefold 1) We want to realize an experimental geometry in which the thermomechanical influence on the thermal effusion can be analytically calculated [13]. 2) The spherical container of the liquid is a piezoelectric spherical shell by which it is possible to measure the adiabatic bulk modulus [14] on the very same sample under identical conditions. 3) The heat conductivity and specific heat can be found independently.

We also in this paper give an account of the 3ω detection technique of our variant.

II. LINEAR RESPONSE THEORY APPLIED TO THERMAL EXPERIMENTS

The experimental method used in this study is, as described in the introduction, an effusion method. A harmonic varying heat current, with angular frequency ω and complex amplitude P , $\text{Re}(Pe^{i\omega t})$, is produced at a surface in contact with the liquid, this heat then “effuses” into the liquid. At the surface a corresponding harmonic temperature oscillation, with complex amplitude δT , $\text{Re}(\delta Te^{i\omega t})$, exists. The current and temperature can be thought of as stimuli and response (but which is which can be interchanged at will), and the two are linearly related if $|P|$ and $|\delta T|$ is small enough. It is hence convenient to introduce the complex frequency-dependent thermal impedance of the liquid

$$Z_{\text{liq}} = \frac{\delta T}{P}. \quad (5)$$

The terminology thermal *impedance* derives naturally from the close analogy between the flow of thermal heat and flow of electricity [15]. Temperature corresponds to electric potential and heat current to electrical current. The analogies also applies to the heat conductivity which corresponds to the specific electric conductivity, and the specific heat which corresponds to electrical capacity.

As an example the thermal impedance of a thermally thin sample is given as

$$Z_{\text{liq,thin}} = \frac{1}{i\omega cV} \quad (6)$$

where c is the volume specific heat and V the volume of the sample. Again an equation completely equivalent to the electrical correspondence between capacitance and impedance.

In the classical case of a planar heater in a thermal thick situation the thermal impedance is found to be [3]

$$Z_{\text{liq,planar}} = \frac{1}{A\sqrt{i\omega c\lambda}} \quad (7)$$

where λ is the thermal conductivity and A the plate area. The lateral dimension W has to be large ($W \gg |l_D(\omega)|$) for this formula to be exact and unfortunately correction terms that take boundary effects into account decays only slowly as $\omega^{-1/2}$ [8]. In the case where the thermal conductivity, λ_s , and specific heat, c_s , of the heater substrate has to be taken into account admittances can be added (in the infinite plate limit), giving

$$Z_{\text{liq,planar}} = \frac{1}{A\sqrt{i\omega c\lambda} + A\sqrt{i\omega c_s\lambda_s}}. \quad (8)$$

III. THERMAL EFFUSION IN SPHERICAL GEOMETRY

Thermal effusion is possible in a spherical geometry as well as in a planar geometry. Imagine a liquid confined between to radii r_1 and r_2 . An imposed oscillating outward heat current $\text{Re}(P(r_1)e^{i\omega t})$ at radius r_1 results in a temperature oscillation $\text{Re}(\delta T(r_1)e^{i\omega t})$ at the same radius. The heat wave propagating out into the liquid gives rise to a coupled strain wave due to thermal expansion. The heat diffusion is thus dependent on the mechanical boundary conditions and mechanical properties of the liquid. It is widely assumed that the transport of heat in a continuum is described by the heat diffusion equation

$$i\omega\delta T = D\nabla^2\delta T \quad (9)$$

where D is a heat-diffusion constant. By the same token one might take the heat diffusion constant as $D = \lambda/c_V$ if the surfaces at r_1 and r_2 are clamped and $D = \lambda/c_p$ if one of the surfaces is free to move. This common belief is not entirely correct. If shear modulus is nonvanishing compared to bulk modulus the description of heat diffusion cannot be decoupled to a bare heat diffusion equation [11, 12, 13, 16]. Such a situation arises dynamically at frequencies where $\omega \approx \frac{1}{\tau_M}$. The fully coupled thermomechanical equations have been discussed in detail, by some of us, in planar geometry in [11] and in spherical geometry in [13]. In general the solutions are complicated but in the case of a spherical geometry where the outer radius r_2 is much larger than the thermal diffusion length, $|l_D(\omega)| \ll r_2$ the solution becomes simple. In terms of the thermal impedance, Z_{liq} , at the inner radius, r_1 , one has

$$Z_{\text{liq}} = \delta T(r_1)/P(r_1) = \frac{1}{4\pi\lambda r_1 \left(1 + \sqrt{i\omega r_1^2 c_l/\lambda}\right)}, \quad (10)$$

It is very interesting that in this thermally thick limit, the thermal impedance is independent of the mechanical boundary conditions [12, 13]. I.e. in the two cases of clamped or free boundary conditions mentioned before it is neither the isochoric nor the isobaric specific heat that enters the diffusion constant and the thermal impedance but the longitudinal specific heat. Since a closed spherical surface has no boundary there are no correction terms like the ones to Eq. (7) discussed above for planar plate effusion. Notice from Eq. (5) that associated with given radius r_1 is a characteristic heat diffusion time

$$\tau_D = r_1^2 c_l/\lambda. \quad (11)$$

When c_l is real the imaginary part of Z_{liq} peaks at $\omega = 1/\tau_D$.

Specific heat measurements in a spherical geometry have earlier been conducted in the thermal thin limit [17]. Here we explore the thermal thick limit (with respect to the outer radius r_2).

IV. $3\omega_e$ -DETECTION TECHNIQUE

The $3\omega_e$ detection technique we use (where the subscript e indicates that it is the electrical angular frequency not the thermal) is different from other $3\omega_e$ techniques (e.g. Ref. [18]) in two ways. Firstly we include higher order terms in the temperature dependency of the thermistor used and in the power oscillations produced. Secondly we use a direct measurement of the time dependent voltage over a voltage divider instead of a lock-in amplifier.

A. The principle.

The $3\omega_e$ -detection technique makes it possible to measure the temperature with the same electrical resistor which generates the heat and thereby at the same location. The principle is in short the following: Applying an electrical current at cyclic frequency ω_e through a resistor a combined constant (zero frequency) and $2\omega_e$ component Joule heating is produced. This gives rise to a combined temperature DC-offset and temperature oscillation at $2\omega_e$, the size of which depends on the thermal environment (the thermal impedance). The resistor is chosen to be temperature dependent, it is a so-called *thermistor*. The temperature oscillations therefore creates a perturbation of the resistance at frequency $2\omega_e$. The voltage across the thermistor which by Ohm's law is the product of current and resistance thus contains a $3\omega_e$ (and an additional $1\omega_e$) component proportional to the temperature oscillations at $2\omega_e$. In practise

one rather has a voltage source than a current source. In order to get a $3\omega_e$ signal the thermistor is therefore placed in series with a temperature independent preresistor as detailed in the following.

The result of the analysis is the frequency dependent thermal impedance at a frequency of $2\omega_e$. It is convenient to express this thermal impedance as function of the frequency of the thermal signal which we designate ω and notice that $\omega = 2\omega_e$.

We first outline the simplest lowest order theory in order to elucidate the technique most clearly. However in order to increase the signal to noise ratio it is expedient to choose a thermistor with a large temperature dependency and to choose temperature amplitudes as high as possible although within the linear regime of the liquid thermal response. This necessitates higher harmonics be taken into account. This detailed analysis is deferred to appendix A.

B. A detour on the complex notation.

In the following we use complex notation for representing the periodic signals. Generally a sum of harmonic terms,

$$A = A_0 + |A_1| \cos(\omega_e t + \phi_1) + \dots + |A_n| \cos(n\omega_e t + \phi_n) \quad (12)$$

with real amplitudes, $A_0, |A_k|$ and phases, ϕ_k can be written as,

$$A = \frac{1}{2} \left(A_0 + A_0 + |A_1| e^{i(\omega_e t + \phi_1)} + |A_1| e^{-i(\omega_e t + \phi_1)} + \dots + |A_n| e^{i(n\omega_e t + \phi_n)} + |A_n| e^{-i(n\omega_e t + \phi_n)} \right). \quad (13)$$

By introducing the complex amplitudes $A_k = |A_k| e^{i\phi_k}$ and the shorthand notation $E_k = e^{ik\omega_e t}$ the sum becomes

$$A = \frac{1}{2} (A_0 + A_1 E_1 + \dots + A_n E_n + c.c.), \quad (14)$$

where $+c.c.$ means that the complex conjugated of all the terms within the parenthesis should be added, including the real constant term. Note that $E_0 = 1$, $E_k E_l = E_{k+l}$, and $E_k E_l^* = E_{k-l}$.

Complex numbers are known to be of great use in harmonic analysis of linear systems. Since the heat current is quadratic in the imposed electrical current and the whole idea of the $3\omega_e$ detection techniques is to exploit the inherent nonlinearity introduced by the temperature dependence of the thermistor the formalism becomes a little more troubled than in pure linear applications. Thus we have to drag around the complex conjugate terms in order to get product terms right. Notice that in products the DC-components get doubled because there is no difference between E_0 and E_0^* , and any product of an n 'th and m 'th harmonic will produce both a $n + m$ 'th and $n - m$ 'th harmonic term.

C. Fundamental equations for the voltage divider

Consider the diagram of Fig. 1. $U(t)$ is the voltage of the source and $V(t)$ the voltage across the temperature independent preresistor, R_{pre} . $U(t)$ and $V(t)$ can be measured directly. $R(T(t))$ is the temperature dependent resistance of the heater/sensor (we will explicit state the temperature/time dependencies when appropriate, otherwise it is implicitly assumed).

The current $I(t)$ through $R(T(t))$ and R_{pre} is given as

$$I(t) = \frac{U(t)}{R_{\text{pre}} + R(T(t))} = \frac{V(t)}{R_{\text{pre}}}, \quad (15)$$

and the power produced in the heater as

$$P(t) = I(t)^2 R(T(t)) = \frac{R(T(t))}{(R_{\text{pre}} + R(T(t)))^2} U(t)^2. \quad (16)$$

Eq. (15) gives the voltage divider equation

$$V(t) = \frac{R_{\text{pre}}}{R_{\text{pre}} + R(T(t))} U(t) \quad (17)$$

which allows for determination of $T(t)$ from the measured voltages.

D. The AC-method to lowest order.

The thermistor and the surrounding sample are placed in a cryostat that defines an overall reference temperature, T_{cryo} . The power produces a (real) temperature change $\Delta T = T - T_{\text{cryo}}$ at the heater/sensor depending on the thermal impedance Z (as defined in section II) the heater/sensor looks into. The temperature rise has a real DC-component, T_0 , and complex AC-components, it can in general be written as:

$$\Delta T = \frac{1}{2}(T_0 + T_1 E_1 + T_2 E_2 + T_3 E_3 + T_4 E_4 + \dots + c.c.) \quad (18)$$

the dominant terms will be the DC component, T_0 , and the second harmonic term, T_2 (see next section).

To first order in the temperature variations the thermistor has a resistance of

$$R = R_0(1 + \alpha_1 \Delta T). \quad (19)$$

Here R_0 and α_1 are considered constant at a given cryostate temperature but they vary with T_{cryo} . In fact the thermistor which is based on a semiconducting material has a resistance that over a larger temperature range is described by

$$R = R_\infty e^{T_a/T}. \quad (20)$$

α_1 is thus related to T_a by

$$\alpha_1 = -\frac{T_a}{T_{\text{cryo}}^2}. \quad (21)$$

Characteristic values of R_∞ and T_a are given in table I.

Substituting Eq. (19) into Eq. (17) we obtain

$$V = \frac{1}{1 + A(1 + \alpha_1 \Delta T)} U \approx \frac{1}{A + 1} (1 - a \Delta T) U \quad (22)$$

where $A = R_0/R_{\text{pre}}$, $a = \frac{A\alpha_1}{1+A}$ and the second expression is to first order in ΔT as also assumed in Eq. 19.

In the simple case, which we first discuss, we assume that the function generator can deliver a pure single harmonic that is

$$U(t) = \frac{1}{2}(U_1 E_1 + c.c.). \quad (23)$$

Eqs. (18) and (23) can now be substituted into Eq. (22).

$$V = \frac{1}{A + 1} \left(1 - a \left(T_0 + \frac{1}{2}(T_1 E_1 + T_2 E_2 + T_3 E_3 + T_4 E_4 + \dots + c.c.) \right) \right) \frac{1}{2}(U_1 E_1 + U_1^* E_1^*). \quad (24)$$

In principle the result contains all harmonics, but it turns out that the interesting ones are the first and third harmonic. The complex amplitudes are by inspection seen to be (remembering that the coefficient to e.g. E_1 is $1/2V_1$, hence a factor a $1/2$ is lost.)

$$V_1 = \frac{1}{A + 1} \left(U_1 - a T_0 U_1 - \frac{1}{2} a T_2 U_1^* \right) \quad (25)$$

and

$$V_3 = \frac{1}{A + 1} \left(-\frac{1}{2} a T_2 U_1 - \frac{1}{2} a T_4 U_1^* \right). \quad (26)$$

Notice that even as ΔT is written as an infinite sum (as in Eq. (18)), one only obtains the included terms. This is a consequence of assuming a perfect voltage source.

If the temperature dependence of the resistance of the thermistor (as expressed through α_1) is not too large the T_4 term can be neglected, leading to

$$V_3 = -\frac{1}{2} \frac{a}{(A+1)} T_2 U_1. \quad (27)$$

Eq. (25) and (27) can finally be solved in T_0 and T_2 as

$$T_2 = -2 \frac{V_3(A+1)}{aU_1} \quad (28a)$$

$$T_0 = -\frac{V_1(A+1) - (U_1 - \frac{1}{2}aT_2U_1^*)}{aU_1}. \quad (28b)$$

The T_0 and T_2 component terms are related to the power through the DC thermal impedance Z_0

$$T_0 = Z_0 P_0 \quad (29)$$

and the complex AC-thermal impedance Z_2 (the impedance at $2\omega_e$)

$$T_2 = Z_2 P_2, \quad (30)$$

with the power also written as a harmonic expansion. In the following section we will show that the power can be found from the measured voltages, and hence that the thermal impedance can be found.

E. Power terms

If the 1. order approximation of the resistance of the thermistor is substituted into the power equation, Eq. (16), the following expression is obtained

$$P = \frac{1}{R_{\text{pre}}} \frac{A(1 + \alpha_1 \Delta T)}{(1 + A(1 + \alpha_1 \Delta T))^2} U^2 \approx \frac{1}{R_{\text{pre}}} \frac{A}{(1 + A)^2} \left(1 + \frac{1 - A}{1 + A} \alpha_1 \Delta T \right) U^2 \quad (31)$$

where the second expression is to first order in ΔT (as generally assumed).

>From this equations it is observed that an input voltage which is a pure 1. harmonic leads to dominant 0. and 2. harmonics in the power/temperature. Notice that if the thermistor resistance were temperature independent, that is $\alpha_1 = 0$, then P_0 equals $|P_2|$ exactly but in general they are almost identical, $P_0 \approx |P_2|$.

It can further be seen that even if the voltage generator is purely single harmonic, the power can have a $4\omega_e$ component from the interplay between the $2\omega_e$ temperature variation and the $2\omega_e$ variation of the squared voltage. In principle further higher harmonics are generated this way. It can however be observed that if α_1 is small, and if $A \approx 1$ which is normally wanted, the higher harmonics will be small (and decreasing with order).

Eq. (31) is not very practical for calculating the power needed for evaluating the thermal impedance from the temperature amplitudes obtained from Eq. (25) and (27), as ΔT is needed.

The power can alternatively be found from

$$P = I(U - V) = \frac{(U - V)V}{R_{\text{pre}}} \quad (32)$$

using Eq. (15). From this equation the power can be determined from directly measured quantities.

If only the $1\omega_e$ component are taken into account the following approximations are obtained

$$P \approx \frac{1}{4R_{\text{pre}}} ((U_1 - V_1)E_1 + c.c.)(V_1E_1 + c.c.) = \frac{1}{4R_{\text{pre}}} ((U_1 - V_1)V_1^* + (U_1 - V_1)V_1E_2 + c.c.) \quad (33)$$

leading to power coefficient given as

$$P_0 = \frac{1}{4R_{\text{pre}}} ((U_1 - V_1)V_1^* + (U_1^* - V_1^*)V_1) \quad (34a)$$

and

$$P_2 = \frac{1}{2R_{\text{pre}}}(U_1 - V_1)V_1. \quad (34b)$$

A more general expansion as given in appendix B, can easily be calculated.

F. Calibration of the thermistor

The characteristics of the thermistor (as expressed through R_0 and α_1) are needed in order to utilize Eq. (27) for finding the thermal impedance.

Eq. (25) can be used for calibrating the temperature dependence of R by finding $A(T_{\text{cryo}})$ at different cryostat temperatures. Roughly we have $V_1 \approx 1/(A+1)U_1$. However due to the finite DC power, P_0 , the DC-temperature is raised the little amount, T_0 , above the cryostat temperature, T_{cryo} , which is the physical reason for the term aT_0U_1 (selfheating). We have that $T_0 = Z_0P_0$, thus in a plot of V_1/U_1 versus P_0 we find A by extrapolation to $P_0 = 0$, assuming that Z_0 is independent of the small temperature changes from the selfheating. This procedure presumes that the third term $\frac{1}{2}aT_2U_1^*$ can be neglected compared to the second term. This can be fulfilled at sufficiently high frequencies, as it can be observed from Eq. (10) that $Z_{\text{liq}} \rightarrow 0$ for $\omega \gg 1/\tau_D$, with $\tau_D = r_1^2 c_l / \lambda$ (in this experiment we have $1/\tau_D \approx 1.88\text{s}^{-1}$ corresponding to a characteristic thermal frequency of $\nu = \left(\frac{1}{2\pi} \frac{1}{\tau_D}\right) \approx 0.3\text{Hz}$).

$A(T_{\text{cryo}})$ is found in this way at a number of temperatures, T_{cryo} , and R_∞ and T_a can then be found by fitting to Eq. (20). α_1 can finally be determined from Eq. (21) at the relevant temperatures.

After this calibration Eqs. (27), (30) and (34b) gives the thermal impedance, Z_2 at $\omega = 2\omega_e$, and Eqs. (25), (29) and (34a) likewise the DC thermal impedance, Z_0 . Agreement should be obtained between $Z_2(\omega)$ for $\omega \rightarrow 0$ and Z_0 .

G. The AC-method refined.

As mentioned earlier we have to do a little more complicated analysis of the detected harmonics of the voltages. These extra terms stem from different sources: 1) The voltage source itself has higher harmonics and a DC-offset. 2) A second order term in the temperature dependence of the thermistor resistance. 3) The $4\omega_e$ Joule power component produced by the $2\omega_e$ variation of the thermistor (as discussed in section IVE). By the analysis we describe below these effects are taken into account.

Regarding point 1) we now write the source voltage, $U(t)$, as

$$U(t) = \frac{1}{2}(U_0 + U_1E_1 + U_2E_2 + U_3E_3 + U_4E_4 + c.c.) \quad (35)$$

including up to the fourth order harmonics. A U_3 component from the source is to be expected since the source itself has an inner resistance. The U_0 is a DC-offset that were present in this experiment but in principle should be eliminated.

Regarding point 2) we now write the temperature dependence of the thermistor as

$$R = R_0(1 + \alpha_1\Delta T(t) + \alpha_2\Delta T(t)^2). \quad (36)$$

Because $R(T)$ follows Eq. (20) over an extended temperature range α_2 and α_1 are connected:

$$\alpha_2 = \frac{\alpha_1^2}{2} - \frac{\alpha_1}{T_{\text{cryo}}}. \quad (37)$$

Point 3) is taken into account by expanding also $V(t)$, $P(t)$ and $T(t)$ like $U(t)$ in Eq. (35) up to the fourth Fourier components.

The analysis can be found in the appendix A. Fortunately it leads to rather simple extensions of the Eqs. (25) and (27). Instead we have

$$V_1 = \frac{1}{A+1} \left[U_1 - aT_0U_1 - \frac{1}{2}aT_2U_1^* + X_1 \right] \quad (38a)$$

and

$$V_3 = \frac{1}{A+1} \left[-\frac{1}{2}aT_2U_1 + U_3 + X_3 \right] \quad (38b)$$

with

$$X_1 = -aT_1U_0 + bT_0^2U_1 + \frac{1}{2}bT_2T_2^*U_1 + bT_0T_2U_1^* \quad (38c)$$

$$X_3 = -\frac{1}{2}aT_4U_1^* + \frac{1}{4}bT_2^2U_1^* + bT_0T_2U_1 \quad (38d)$$

where $a = \frac{A\alpha_1}{1+A}$ and $b = \left(\frac{A\alpha_1}{1+A}\right)^2 - \frac{A\alpha_2}{1+A}$, and only terms larger than $5 \cdot 10^{-7}U_1$ are included.

The two important power components are calculated from the V_i 's and U_i 's as in Eq. (34) by

$$P_0 = \frac{1}{R_{\text{pre}}} \left(W_0V_0 + \frac{1}{2}\text{Re}(W_1V_1^* + W_2V_2^* + W_3V_3^* + W_4V_4^*) \right) \quad (39)$$

and

$$P_2 = \frac{1}{R_{\text{pre}}} \left(W_0V_2 + W_2V_0 + \frac{1}{2}(W_1V_1 + W_1^*V_3 + W_2^*V_4 + W_3V_1^* + W_4V_2^*) \right) \quad (40)$$

where $W = U - V$. The full set of power components are given in Eq. (B1).

The coupled Eqs. (38a) and (38b), that are nonlinear in T_0 and T_2 , can be solved by iteration. We rewrite them as

$$T_0 = -\frac{V_1(A+1) - (U_1 - \frac{1}{2}aT_2U_1^* + X_1)}{aU_1} \quad (41a)$$

$$T_2 = -2\frac{V_3(A+1) - (U_3 + X_3)}{aU_1}. \quad (41b)$$

We start by putting $X_1 = X_3 = 0$ and evaluate Eq. (41b) getting a T_2 which is equal to the first order solution Eq. (27) (including correction for a possible direct $3\omega_e$ signal from the generator), after which Eq. (41a) can be evaluated to give the exact solution of Eq. (25).

A provisory thermal impedance $Z_2 = T_2/P_2$ is found. Then $T_1 = Z_1P_1$ and $T_4 = Z_4P_4$ can be estimated since $Z_1(\omega) = Z_2(\omega/2)$ and $Z_4(\omega) = Z_2(2\omega)$. The perturbative terms, X_1, X_3 , can then be found and with these values in Eqs. (41a) and (41b) a better estimation of T_0 and T_2 is found. This process is iterated until convergence. The pair of equations Eq. (38) can alternatively be solved for A and T_2 , which by an equivalent iterative method provides better values for A . By altering between the two sets of solutions and iterating the equations, full convergence is obtained.

V. EXPERIMENTAL

The measurements were performed using a custom built setup [19, 20]. The temperature is controlled by a custom built cryostat with temperature fluctuations smaller than 2mK (see Ref. 19 for details on the cryostat). The electrical signals were measured using a HP3458A multimeter in connection with a custom-built frequency generator as sketched on Fig. 1 (see Ref. [20] for details on the electrical setup, but notice that in this experiment we use the generator and multimeter in a slightly altered configuration). The electrical setup allows for measurements in the frequency (ν_e) range from 1mHz up to 100Hz.

The used thermistor was of the type U23UD from Bowthorpe Thermometrics, and was positioned in the middle of a sphere as shown on Fig. 2. The details of the sphere is as discussed earlier unimportant, and in this case the

piezoelectric bulk transducer [14] is used as such. The sphere is filled at room temperature with additional liquid in the reservoir. This additional liquid ensures that the sphere stay complete filled as it is cooled to the relevant temperature.

The liquid investigated was a five-ring polyphenyl ether (5-polyphenyl-4-ether) the Santovac® 5 vacuum pump fluid (CAS number 2455-71-2). The liquid was used as received, without further purification.

Data were taken as frequency scans at constant temperature, with the liquid in thermal equilibrium. The direct output from the frequency generator was measured, under electrical load, at each sample temperature before measuring the voltage over the preresistor, to eliminate any long term drifts in the frequency generator. The measurements were furthermore carried out at two different input amplitudes, $\langle |U_1| \rangle \approx 4.9\text{V}$ and $\langle |U_1| \rangle \approx 2.9\text{V}$, to allowing for a test of the inversion algorithm and linearity of the final thermal response. All results presented in this paper is from the larger of the two amplitudes if not stated otherwise. To test for reproducibility and equilibrium some of the measurements were retaken during the reheating of the sample. The outcome of the measurements are the complex amplitudes $U_i(\nu_e)$ and $V_i(\nu_e)$ for the harmonics of the voltages U and V .

Table I gives the key experimental parameters for the measurements at the high input amplitude.

VI. DATA ANALYSIS

In the following we denote the measured thermal impedance Z_2 by simply Z dropping the subscript 2. The subscripts were practical in the technical description of the detection method indicating that the thermal impedance is found at a thermal frequency ω which is the double of the electrical frequency ω_e . But in discussing the thermal properties of liquids only the thermal frequency $\omega = 2\pi\nu$ is relevant. The temperature we refer to at which a measurement is done is the mean temperature $T = T_0 + T_{\text{cryo}}$.

The thermal impedance has been calculated from the measured voltage harmonics using the scheme described above. As an example the absolute value of Z as a function of frequency, ν , is shown in Fig. 3 at $T = 295.6\text{K}$, where the liquid shows no relaxation. The thermal impedance has been measured at two different input voltage amplitudes U_1 of the voltage divider of Fig. 1 and thus at two different power amplitudes. The liquid thermal response, the temperature, is expected to be linear in the power amplitudes and thus the thermal impedance should be independent of the power amplitude. This is seen to be fulfilled for the thermal impedance, Z , from the elaborated analysis of section IV. The 1.order analysis however is seen to give a power dependent thermal impedance demonstrating the necessity of taking into account the higher order terms of the elaborated analysis (as described in section IV G).

Figure 4 shows the real and imaginary part of the thermal impedance, Z , in a log-log plot at 295.6K. The measured impedance has more features than predicted by the simple expression for the thermal impedance of spherical effusion (Eq. 10). For example the high frequency behavior should be characterized by a line of slope 1/2 but this is seen not to be the case. The additional features come from thermal properties of the thermistor bead, the influence of which we are going to study below. We stress that although Z shows dispersion and has a real and imaginary part this has nothing to do with liquid relaxation — which is absent at this temperature — but is only a consequence of heat diffusion in spherical geometry. However relaxation should of course affect the thermal impedance. This is shown in Fig. 5 where Z at 252.7K and 256.7K are compared. The glass transition is seen to give only a slight perturbation of the shape of the Z -curve. In order to obtain any reliable specific heat data from the thermal impedance it is thus imperative to have an accurate model of the thermal interaction between liquid and thermistor bead.

The bead (see Fig. 6) consist of a core of radius r_0 , where the temperature amplitude $\delta T(r_0)$ is actually measured and the heat current $P(r_0)$ generated. This core is surrounded by a glass capsule of outer radius r_1 , at which the bead is in contact with the liquid. The heat flow $P(r_1)$ out through the surface at r_1 is in general different from $P(r_0)$ and also the temperature $\delta T(r_1)$ can be different from $\delta T(r_0)$. Now the liquid thermal impedance is

$$Z_{\text{liq}} = \frac{\delta T(r_1)}{P(r_1)} \quad (42)$$

whereas the measured thermal impedance is rather

$$Z = \frac{\delta T(r_0)}{P(r_0)}. \quad (43)$$

The capsule layer has a heat conductivity λ_b and a specific heat c_b . The heat diffusion constant becomes $D_b = \lambda_b/c_b$ and the thermal wavevector $k_b = \sqrt{i\omega/D_b}$. The bead is a solid for which in general the difference between the

isobaric and isochoric specific heats are small, and are frequency independent. The heat diffusion through this shell is thus well described [13] by a thermal transfermatrix $\mathbf{T}^{\text{th}}(\lambda_b, c_b, r_1, r_0)$

$$\begin{pmatrix} \delta T(r_1) \\ P(r_1)/(i\omega) \end{pmatrix} = \mathbf{T}^{\text{th}}(r_1, r_0) \begin{pmatrix} \delta T(r_0) \\ P(r_0)/(i\omega) \end{pmatrix}. \quad (44a)$$

The components of $\mathbf{T}^{\text{th}}(r_1, r_0)$ are given by [13]

$$T_{11}^{\text{th}}(r_1, r_0) = \frac{r_0}{r_1} \cosh(k_b(r_1 - r_0)) + \frac{1}{k_b r_1} \sinh(k_b(r_1 - r_0)) \quad (44b)$$

$$T_{12}^{\text{th}}(r_1, r_0) = -\frac{i\omega}{4\pi\lambda_b} \frac{\sinh(k_b(r_1 - r_0))}{k_b r_0 r_1} \quad (44c)$$

$$T_{21}^{\text{th}}(r_1, r_0) = \frac{4\pi c_b}{k_b^3} \left[(1 - k_b^2 r_0 r_1) \sinh(k_b(r_1 - r_0)) - k_b(r_1 - r_0) \cosh(k_b(r_1 - r_0)) \right] \quad (44d)$$

$$T_{22}^{\text{th}}(r_1, r_0) = \frac{r_1}{r_0} \cosh(k_b(r_1 - r_0)) - \frac{1}{k_b r_0} \sinh(k_b(r_1 - r_0)). \quad (44e)$$

Combining Eqs. (42), (43) and (44a) one finds that the measured thermal impedance, Z , is related to the liquid thermal impedance, Z_{liq} , as

$$Z_{\text{liq}} = \frac{1}{i\omega} \frac{T_{11}^{\text{th}}(r_1, r_0)i\omega Z + T_{12}^{\text{th}}(r_1, r_0)}{T_{21}^{\text{th}}(r_1, r_0)i\omega Z + T_{22}^{\text{th}}(r_1, r_0)}. \quad (45)$$

Conversely, since $\mathbf{T}^{\text{th}-1}(r_1, r_0) = \mathbf{T}^{\text{th}}(r_0, r_1)$ [13] the inverse relation is

$$Z = \frac{1}{i\omega} \frac{T_{11}^{\text{th}}(r_0, r_1)i\omega Z_{\text{liq}} + T_{12}^{\text{th}}(r_0, r_1)}{T_{21}^{\text{th}}(r_0, r_1)i\omega Z_{\text{liq}} + T_{22}^{\text{th}}(r_0, r_1)}. \quad (46)$$

In order to get Z_{liq} from the measured Z one has to know the parameters r_0, r_1, λ_b and c_b characterizing the thermal structure of the intervening thermistor bead. These four parameters are determined in the following way.

First r_0 and r_1 are found. At each temperature the measured thermal impedance, Z , is fitted by the formula (46) including the expression given in Eq. (10) for Z_{liq} . These fits involve the six frequency independent fitting parameters $r_0, r_1, \lambda_b, c_b, \lambda$ and c_l . The result for r_0 and r_1 is seen in Fig. 7. Measurements were taken both going downwards to the glass transition and upwards again to room temperature. In the glass transition range where the liquid specific heat, c_l , is expected to be complex and frequency dependent these fits of course doesn't work. This is the reason for the scatter of data at low temperature. However at higher temperatures r_0 and r_1 are meaningfully found. For a reasonable expansion coefficient of the bead material these radii hardly changing more than 0.1% going 100K below room temperature. Thus we will consider r_0 and r_1 as temperature independent and they are found as their mean values above the glass transition range (shown as solid lines in Fig. 7). We find $r_0 = 0.114\text{mm}$ and $r_1 = 0.206\text{mm}$. Data has also been processed for the lower input amplitude resulting in a change of r_0 below 1% and r_1 below 0.1%.

Secondly, with the fixed values of r_0 and r_1 the thermal impedance data, Z , are again fitted as a function of the four frequency independent fitting parameters λ_b, c_b, λ and c_l . This two step fitting algorithm gives smaller scatter in these parameters and is reasonable because r_0 and r_1 is known to have insignificant temperature dependencies.

The solid line in Fig. 4 shows the result of such a fit to Z -data at room temperature (295.6K) The model captures the features in the frequency dependence of the measured thermal impedance very precisely. In table II we report the results for λ_b, c_b, λ and c_l , obtained at room temperature. Four values are given for each quantity, they are taken at the two input amplitudes and from a initial measurement at room temperature and a measurement taken at the end of the temperature scan. The method is seen to give very reproducible results.

According to the specifications for Santovac® 5 given by Scientific instrument service, Inc [21] the value of λ at 20°C is 0.1330W/(K·m). They likewise report the isobaric specific heat pr. mass $c_p/\rho = 0.35\text{cal}/(\text{g} \cdot \text{K})$ and density $\rho = 1.204\text{g}/\text{cm}^3$ at 20°C giving a specific heat pr. volume of $c_p = 1.76 \cdot 10^6 \text{J}/(\text{K} \cdot \text{m}^3)$. These values must be considered equal to ours within limits of error. Note that at these temperatures the isobaric and longitudinal specific heats are identical. Also in Fig. 4 is shown the thermal impedance as it would have been if the properties of the thermistor bead itself had been negligible, i.e. if Z was identical to Z_{liq} of Eq. (10) We note that especially the high frequency

behaviors are different but also the limiting value at low frequency is higher for the measured Z than for Z_{liq} . This is due to the additional thermal resistance in the bead capsule layer.

The result for the heat conductivity and specific heat of the glass capsule of the thermistor bead, λ_b and c_b , as a function of temperature is shown in Fig. 8. Again of course the fitting is only meaningful above the glass transition temperature range. However we need to know λ_b and c_b in this range as well. The weak temperature dependencies of these quantities are thus fitted to linear functions above the glass the transition range (shown as solid lines in Fig. 8). The results of the fitting procedures are given in table I.

The extrapolations of λ_b and c_b down in the glass transition range together with the values of r_0 and r_1 can now be used in the inverse formula Eq. (45) for calculating Z_{liq} from the measured thermal impedance. In Fig. 9 the thermal impedance of the liquid, Z_{liq} , and the raw measured thermal impedance, Z , are shown for data taken at room temperature ($= 295.6\text{K}$). As discussed earlier effusion from a plane plate can only give the effusivity $e = \sqrt{\lambda c}$. Thus the specific heat cannot be found absolutely. In contrast effusion from a sphere is able to give both the heat conductivity and the longitudinal specific heat absolutely even if the latter is frequency dependent. However the heat conductivity has to be frequency independent to allow for this separation. The separation is possible because Z_{liq} as given in Eq. (10) has the low frequency limiting value $1/(\sqrt{4\pi\lambda r_1})$. The convergence is rather slow involving the squareroot of the frequency. However if we look at the reciprocal quantity, the thermal admittance $Y_{\text{liq}} = 1/Z_{\text{liq}}$

$$Y_{\text{liq}} = 4\pi\lambda r_1 \left(1 + \sqrt{i\omega r_1^2 c_l / \lambda} \right) \quad (47)$$

we observe that when c_l is frequency independent the squareroot frequency term can be cancelled by taking the difference between Y'_{liq} and Y''_{liq}

$$\lambda = \frac{Y'_{\text{liq}} - Y''_{\text{liq}}}{4\pi r_1}. \quad (48)$$

This is valid even in the glass transition range at sufficiently low frequencies where c_l reaches its non-complex equilibrium value. Figure 10 shows how the temperature dependency of the heat conductivity, λ , of the sample liquid is found by this method. Finally using these values the frequency dependent longitudinal specific heat is calculated from

$$c_l(\omega) = \frac{\lambda}{i\omega r_1^2} \left(\frac{Y_{\text{liq}}}{4\pi\lambda r_1} - 1 \right)^2 \quad (49)$$

In Fig. 11 is shown the result of this data treatment for a number of temperatures.

VII. DISCUSSION

The derived longitudinal specific heat displayed in Fig. 11 shows the expected relaxation phenomena at the glass transition. At 252.7K c_l decreases from $c_0 = c_l(\omega \rightarrow 0) = 1.82 \cdot 10^6 \text{J}/(\text{K} \cdot \text{m}^3)$ to $c_\infty = c_l(\omega \rightarrow \infty) = 1.37 \cdot 10^6 \text{J}/(\text{K} \cdot \text{m}^3)$. The temperature dependency of c_0 above the glass transition range is shown in Fig. 12. The relaxation spectrum may be described by a symmetric Cole-Cole relaxation function $c_l(\omega) = c_\infty + (c_0 - c_\infty)/(1 + (i\omega\tau)^\alpha)$ with an exponent $\alpha = 0.9$. This fit serves to determine the loss peak frequency. The temperature dependency of τ is shown in Fig. 13. However we will not claim the value of the exponent nor the shape of the relaxation curve to be very precise. The high temperature data are seen to show spurious frequency dependency in both the real and imaginary part of c_l . This may be attributed to small systematic errors in the data processing or data acquisition that we have not been able to trace yet. Due to the functional relationship, Eq. (10) between Z_{liq} and c_l a small relative error $|dZ_{\text{liq}}/Z_{\text{liq}}|$ in the thermal impedance may propagate to a large relative error $|dc_l/c_l|$ in the specific heat. As a function of the dimensionless Laplace-frequency $s = i\omega\tau_D$ one finds

$$\frac{dc_l}{c_l} / \frac{dZ_{\text{liq}}}{Z_{\text{liq}}} = 2 \frac{1 + \sqrt{s}}{\sqrt{s}}. \quad (50)$$

This factor is four at the characteristic heat diffusion frequency ($s = 1$) increasing to a factor of 22 at 0.01 times this frequency. Thus the specific heat is difficult to get reliably more than 2 decades below the characteristic diffusion frequency. On the other hand one decade above this frequency the measured Z is dominated by the thermal structure of the thermistor bead that can only be reliably modelled to some extent.

VIII. CONCLUSION

From a theoretical point of view determination of the frequency dependent specific heat from thermal effusion from a sphere has many ideal features. The surface of a sphere — being closed — has no boundary and thus no associated boundary effects like a finite plane plate. The thermomechanical coupling problem can be treated analytically i.e. the influence of the increasing dynamic shear modulus and the mechanical boundary conditions is adequately taken into account. Although the thermomechanical problem can also be solved in the onedimensional unilateral case it is not so obvious whether it really applies to the experimental finite plate realizations. It is of course preferable if thermal experiments can give two independent thermal properties say the specific heat and the heat conductivity or the effusivity and diffusivity. Effusion experiments in different geometries can give the effusivity only unless a characteristic length scale comes into play with the heat diffusion length. For the infinite plane there is no such length scale whereas in the spherical case this length scale is the radius of the heat producing sphere. This advantage is however also the weakness of the method since it limits the practical frequency window to be studied.

Acknowledgments

This work was supported by the Danish National Research Foundation's DNRF center for viscous liquid dynamics "Glass and Time".

APPENDIX A: THE AC-METHOD TO HIGHER ORDER

In this appendix we analyze which higher order terms must be included in order to get a relative accuracy of $1 \cdot 10^{-4}$ on the measured temperature amplitude from the Fourier components of the measured voltages of the voltage divider (see Fig. 1).

In the following we will include up to fourth harmonics in all the relevant quantities, hence we write

$$V(t) = \frac{1}{2} (V_0 + V_1 E_1 + V_2 E_2 + V_3 E_3 + V_4 E_4 + c.c.) \quad (\text{A1a})$$

$$U(t) = \frac{1}{2} (U_0 + U_1 E_1 + U_2 E_2 + U_3 E_3 + U_4 E_4 + c.c.) \quad (\text{A1b})$$

$$P(t) = \frac{1}{2} (P_0 + P_1 E_1 + P_2 E_2 + P_3 E_3 + P_4 E_4 + c.c.) \quad (\text{A1c})$$

$$\Delta T(t) = \frac{1}{2} (T_0 + T_1 E_1 + T_2 E_2 + T_3 E_3 + T_4 E_4 + c.c.). \quad (\text{A1d})$$

Combining the expansion of the thermistor resistance to second order, Eq. (36), with the voltage divider equation, Eq. (17), the voltage across the preresistor becomes, to second order in ΔT ,

$$V(t) = \frac{1}{A+1} (1 - a\Delta T + b\Delta T^2) U \quad (\text{A2})$$

with $A = R_0/R_{\text{pre}}$, $a = \frac{A\alpha_1}{1+A}$ and $b = \left(\frac{A\alpha_1}{1+A}\right)^2 - \frac{A\alpha_2}{1+A}$.

If this expression is explicitly calculated using the above expansions of U and T (Eq. (A1b) and (A1d)) a large number of terms is obtained. In the following we make a numerical inspection of which terms are most significant, in a worst case, to reduce the number of terms included.

In order to calculate the order of magnitude of the terms, an estimate of the size of the components of U and ΔT are needed. In Fig. 14 we show the relative magnitudes of the different components of the input voltage, U , of the voltage divider to U_1 . In table III we summarize the upper limits of these ratios. In Fig. 15 we show the relative magnitude of the different components of the power calculated from the measured U_i and V_i components. In table IV we summarize the upper limits on these ratios. We estimate the relative size of the temperature amplitudes as equal to the relative sizes of the power amplitudes. In table V we give characteristic values of the quantities describing the thermistor and the resistors.

Combing the estimates given in table V, with Eq. (27), we observe that a change in T_2 of $1 \cdot 10^{-4}$ K corresponds to a change in V_3/U_1 of $5 \cdot 10^{-7}$. Hence only terms in the expansion of Eq. (A2) which are larger than $5 \cdot 10^{-7}U_1$ will be included.

By explicit substitution of Eq. (A1b) and (A1d) into Eq. (A2) and insertion of the estimates from table III, IV and V the following expressions are found for the first and third harmonics on the voltage, V , when disregarding terms smaller than $5 \cdot 10^{-7}U_1$

$$V_1 = \frac{1}{A+1} \left[U_1 - aT_0U_1 - \frac{1}{2}aT_2U_1^* + X_1 \right] \quad (\text{A3a})$$

and

$$V_3 = \frac{1}{A+1} \left[-\frac{1}{2}aT_2U_1 + U_3 + X_3 \right] \quad (\text{A3b})$$

with

$$X_1 = -aT_1U_0 + bT_0^2U_1 + \frac{1}{2}bT_2T_2^*U_1 + bT_0T_2U_1^* \quad (\text{A3c})$$

$$X_3 = -\frac{1}{2}aT_4U_1^* + \frac{1}{4}bT_2^2U_1^* + bT_0T_2U_1. \quad (\text{A3d})$$

APPENDIX B: POWER TERMS TO HIGHER ORDER

The relevant set of power components are calculated from Eq. (32) as

$$P = \frac{(U - V)V}{R_{\text{pre}}}$$

using the expansions in Eq. (A1a) and (A1b) to be

$$P_0 = \frac{1}{R_{\text{pre}}} \left(W_0V_0 + \frac{1}{2}\text{Re}(W_1V_1^* + W_2V_2^* + W_3V_3^* + W_4V_4^*) \right) \quad (\text{B1a})$$

$$P_1 = \frac{1}{R_{\text{pre}}} \left(W_1V_0 + V_1W_0 + \frac{1}{2}(W_2V_1^* + W_1^*V_2 + W_3V_2^* + W_2^*V_3 + W_3^*V_4 + W_4V_3^*) \right) \quad (\text{B1b})$$

$$P_2 = \frac{1}{R_{\text{pre}}} \left(W_0V_2 + W_2V_0 + \frac{1}{2}(W_1V_1 + W_1^*V_3 + W_2^*V_4 + W_3V_1^* + W_4V_2^*) \right) \quad (\text{B1c})$$

$$P_3 = \frac{1}{R_{\text{pre}}} \left(W_0V_3 + W_3V_0 + \frac{1}{2}(W_1V_2 + W_2V_1 + W_1^*V_4 + W_4V_1^*) \right) \quad (\text{B1d})$$

$$P_4 = \frac{1}{R_{\text{pre}}} \left(W_0V_4 + W_4V_0 + \frac{1}{2}(W_1V_3 + W_2V_2 + W_3V_1) \right) \quad (\text{B1e})$$

where $W = U - V$.

* Electronic address: tec@ruc.dk

- [1] G. Harrison, *The Dynamic Properties of Supercooled Liquids* (Academic, New York, 1976).
- [2] R. O. Davies and G. O. Jones, *Adv. Phys.* **2**, 370 (1953).
- [3] N. O. Birge and S. R. Nagel, *Phys. Rev. Lett.* **54**, 2674 (1985).
- [4] T. Christensen, *J. Phys. (Paris) Colloq.* **46**, C8-635 (1985).
- [5] H. Huth, A. A. Minakov, A. Serghei, F. Kremer, and C. Schick, *Eur. Phys. J. Special Topics* **141**, 153 (2007).
- [6] N. O. Birge, *Phys. Rev. B* **34**, 1631 (1986).
- [7] I. K. Moon, Y. H. Jeong, and S. I. Kwun, *Rev. Sci. Instrum.* **67**, 29 (1996).

- [8] N. O. Birge, P. K. Dixon, and N. Menon, *Thermochim. Acta* **304-305**, 51 (1997).
- [9] A. A. Minakov, S. A. Adamovsky, and C. Schick, *Thermochim. Acta* **377**, 173 (2001).
- [10] A. A. Minakov, S. A. Adamovsky, and C. Schick, *Thermochim. Acta* **403**, 89 (2003).
- [11] T. Christensen, N. B. Olsen, and J. C. Dyre, *Phys. Rev. E* **75**, 041502 (2007).
- [12] T. Christensen, N. B. Olsen, and J. C. Dyre, in *5th International Workshop on Complex Systems*, edited by M. Tokuyama, I. Oppenheim, and H. Nishiyama (AIP, Melville, NY, 2008, 2008), vol. 982 of *AIP Conf. Proc.*, p. 139.
- [13] T. Christensen and J. C. Dyre, *Phys. Rev. E* **78**, 021501 (2008).
- [14] T. Christensen and N. B. Olsen, *Phys. Rev. B* **49**, 15396 (1994).
- [15] H. S. Carslaw and J. C. Jaeger, *Conduction of heat in solids* (Clarendon Press, Oxford, 1959).
- [16] L. D. Landau and E. M. Lifshitz, *Theory of Elasticity* (Pergamon, London, 1986), 3rd ed.
- [17] T. Christensen and N. B. Olsen, *J. Non-Cryst. Solids* **235-237**, 296 (1998).
- [18] N. O. Birge and S. R. Nagel, *Rev. Sci. Instrum.* **58**, 1464 (1987).
- [19] B. Igarashi, T. Christensen, E. H. Larsen, N. B. Olsen, I. H. Pedersen, T. Rasmussen, and J. C. Dyre, *Rev. Sci. Instrum.* **79**, 045105 (2008).
- [20] B. Igarashi, T. Christensen, E. H. Larsen, N. B. Olsen, I. H. Pedersen, T. Rasmussen, and J. C. Dyre, *Rev. Sci. Instrum.* **79**, 045106 (2008).
- [21] Scientific instrument service, Inc, *Specifications for santovac 5 and santovac 5p ultra*, Web page (2008), URL <http://www.sisweb.com/catalog/08/F14>.

TABLE I: Experimental parameters. **Top:** Parameters characterizing the resistors in the setup, R_{pre} is the resistance of the preresistor, R_∞ and T_a the characteristics of the thermistor according to Eq. (20)). **Middle:** Parameters characterizing the glass capsule of the thermistor bead, r_0 and r_1 is the inner and outer radius, λ_b and c_b is the heat conductivity and specific heat respectively. **Bottom:** Applied amplitudes expressed as mean applied voltage ($\langle |U_1| \rangle$) and maximum temperature amplitude ($\max(|T_2|)_{\nu, T}$).

R_{pre}	3884.3 Ω
R_∞	0.1187 Ω
T_a	2817.9K
r_0	0.114mm
r_1	0.205mm
$\lambda_b(T[K])$	$-3.2 \cdot 10^{-4}T + 1.0517$ [W/(K · m)]
$c_b(T[K])$	$2.9 \cdot 10^{-3}T + 0.7709$ [10^6 J/(m ³ · K)]
$\langle U_1 \rangle_\nu$	4.909V
$\max(T_2)_{\nu, T}$	2.257K

TABLE II: Heat conductivity and specific heat of the glass encapsulation of the thermistor bead (λ_b and c_b), and for the liquid (λ and c_l). The results are at room temperature (295.6K), and taken using two input amplitudes $|U_1|$. The two scans are the initial scan and a scan taken after the temperature scan coming back to room temperature.

$ U_1 $ [V]	P_2 [mW]	scan	λ_b [W/(K · m)]	c_b [10^6 J/(K · m ³)]	λ [W/(K · m)]	c_l [10^6 J/(K · m ³)]
4.9	0.63	1	0.9562	1.6365	0.14002	1.8187
		2	0.9558	1.6370	0.14004	1.8190
2.9	0.23	1	0.9771	1.6261	0.13995	1.8033
		2	0.9763	1.6281	0.13997	1.8033

TABLE III: Maximum of relative magnitude of the components of input voltage U to the dominant first harmonic U_1 , as shown on Fig. 14 (for $\nu < 40$ Hz).

U_0/U_1	U_2/U_1	U_3/U_1	U_4/U_1
$2 \cdot 10^{-2}$	10^{-4}	10^{-5}	$3 \cdot 10^{-5}$

TABLE IV: Maximum of relative magnitude of the components of the power as shown on Fig. 15, (for $\nu < 40$ Hz).

P_0/P_2	P_1/P_2	P_3/P_2	P_4/P_2
1	10^{-1}	10^{-3}	10^{-2}

TABLE V: Characteristic sizes of the parameters describing the used thermistor at $T_{cryo} = 249.5$ K

A	α_1	α_2
≈ 2	$\approx 4 \cdot 10^{-2} \text{K}^{-1}$	$\approx 10^{-3} \text{K}^{-2}$

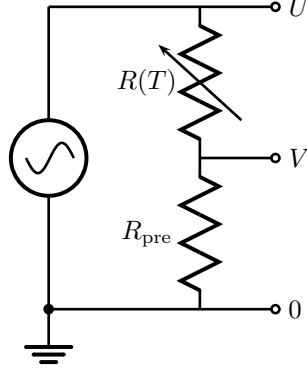


FIG. 1: Voltage divider for the $3\omega_e$ -detection technique. The temperature-dependent resistor (the thermistor) $R(T(t))$ is in thermal contact with the liquid probing its thermal impedance at $2\omega_e$. The preresistor, R_{pre} , is temperature-independent.

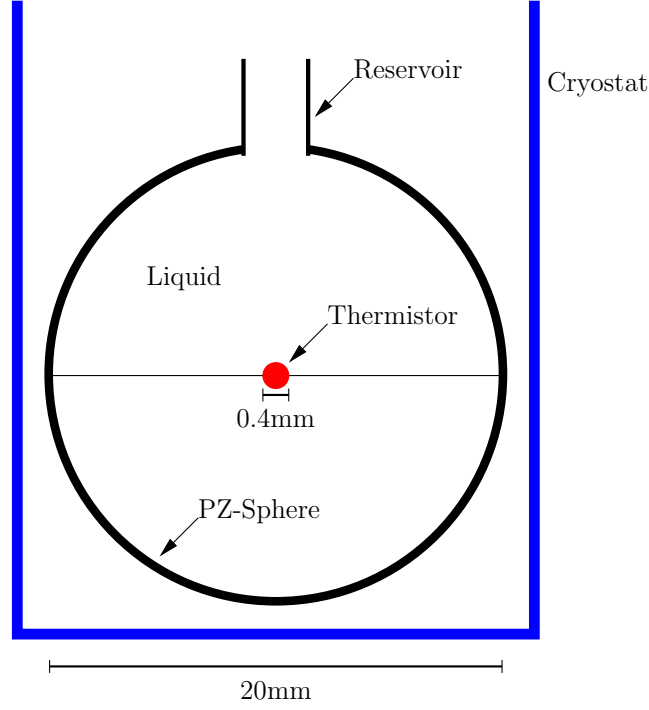


FIG. 2: Schematic illustration of the measuring setup. The thermistor acting as combined heater and thermometer is placed in a sphere filled with the liquid, which is itself placed in a cryostat.

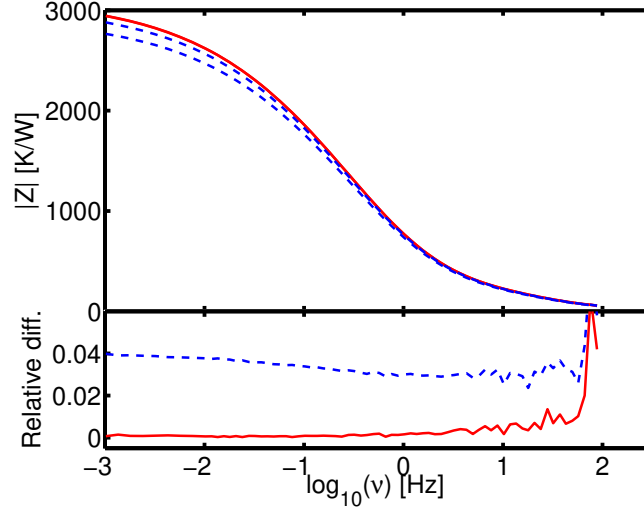


FIG. 3: Comparison of the thermal impedance, Z , obtained from the measurements at two different amplitudes ($\langle U_1 \rangle = 4.9\text{V}$ and 2.9V), and from using the 1. order model as given in Eq. (28) and higher order model as given in Eq. (41) (as described in section IV D and IV G). Data were taken at $T = 295.6\text{K}$. **Top part** shows the raw impedance, notice that there are two full lines, but that they are on top of each other. **Bottom part** shows the relative difference between the two amplitudes ($|Z_{\text{amp}=4.9\text{V}} - Z_{\text{amp}=2.9\text{V}}|/|Z_{\text{amp}=2.9\text{V}}|$). **Dashed lines:** Z calculated from 1. order expression, Eq. (28). **Full lines:** Z calculated from expression including higher order terms, Eq. (41).

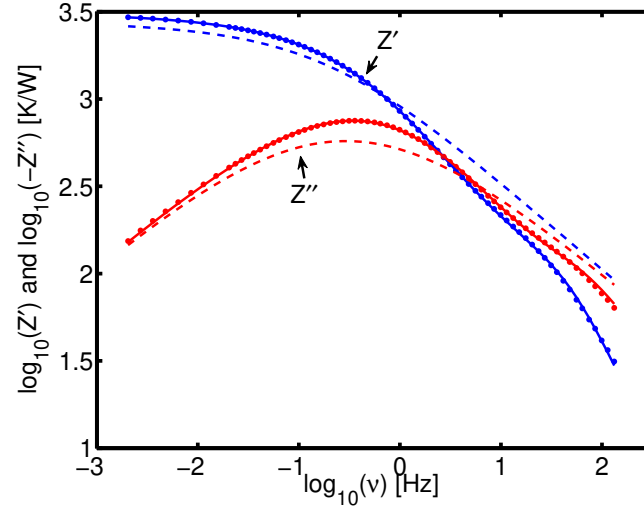


FIG. 4: Comparison of measured thermal impedance, Z , with the result from fitting the full model of liquid and thermistor (Eq. (46) together with Eq. (10)), and the simple model of Z_{liq} (Eq. (10)). The parameters used in evaluation of the simple model are the ones found from the full analysis. Data are taken at room temperature ($T = 295.6\text{K}$). **Dots:** measured points. **Full lines:** full model of liquid and thermistor bead. **Dashed lines** simple model including only liquid.

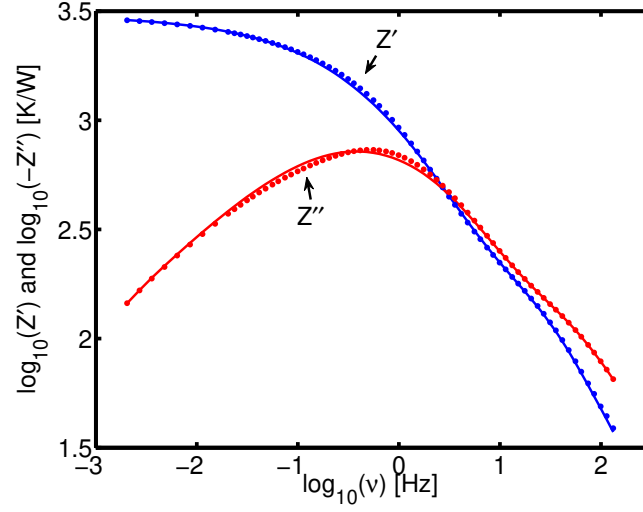


FIG. 5: Comparison of thermal impedance, Z , at two temperatures, showing the small difference due to the frequency dependent specific heat of the liquid, c_l . **Lines:** $T = 256.7\text{K}$. **Dots** $T = 252.7\text{K}$.

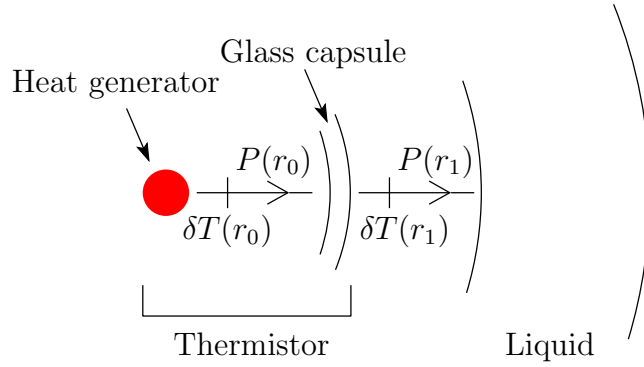


FIG. 6: Schematic thermal network model of the thermistor bead and liquid. The thermal current P and temperature δT are indicated at the inner radius, r_0 , at the border between the heater and the glass capsule and at the outer radius, r_1 , at the border between the glass capsule and the liquid. The thermal impedance of the liquid is defined as $Z_{\text{liq}} = \delta T(r_1)/P(r_1)$. The thermal impedance seen from the thermistor is $Z = \delta T(r_0)/P(r_0)$. The two are connected by Eq. (45) and (46), utilizing the thermal transfermatrix Eq. (44).

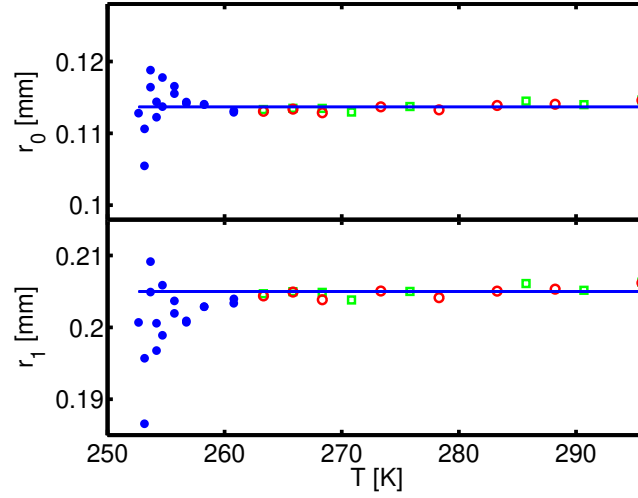


FIG. 7: The inner and outer radii, r_0 and r_1 of the encapsulation of the thermistor-bead. r_0 and r_1 are found at each temperature by fitting the measured thermal impedance, Z , to the 6-parameter thermal network model (Fig. 6) of the spherical heat effusion experiment (Eq. (46) combined with Eq. (10)). **Open squares:** Data taken going down in temperature. **Open circles:** Data taken going up in temperature. **Closed circles:** Low temperature data including points taken going down and up. **Line:** Mean value of the radii found above the liquid glass transition temperature range (open symbols) defines the used radii (see also table I).

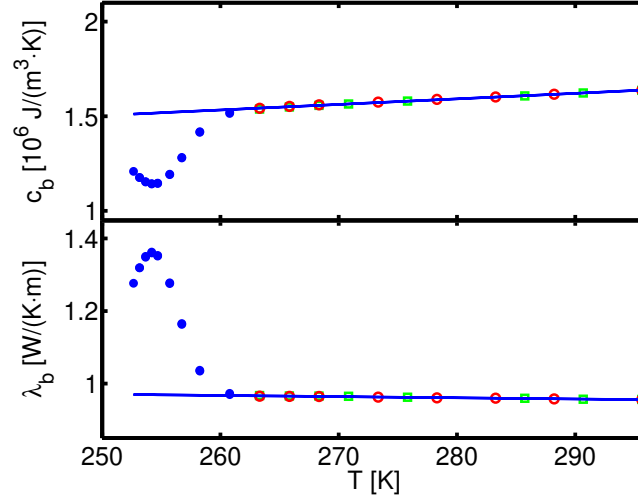


FIG. 8: The specific heat, c_b , and the heat conductivity, λ_b , of the encapsulation of the thermistor-bead. c_b and λ_b are found at each temperature by fitting the thermal network model (Eq. (46) combined with Eq. (10)) to the measured thermal impedance, Z , keeping radii of the bead, r_0 and r_1 , fixed (as given in table I). **Open squares:** Data taken going down in temperature. **Open circles:** Data taken going up in temperature. **Closed circles:** Low temperature data including points taken going down and up. **Line:** Interpolated linear temperature dependencies of c_b and λ_b found above the liquid glass transition temperature range, used for extrapolating down in the region where the liquid relaxation sets in (see also table I).

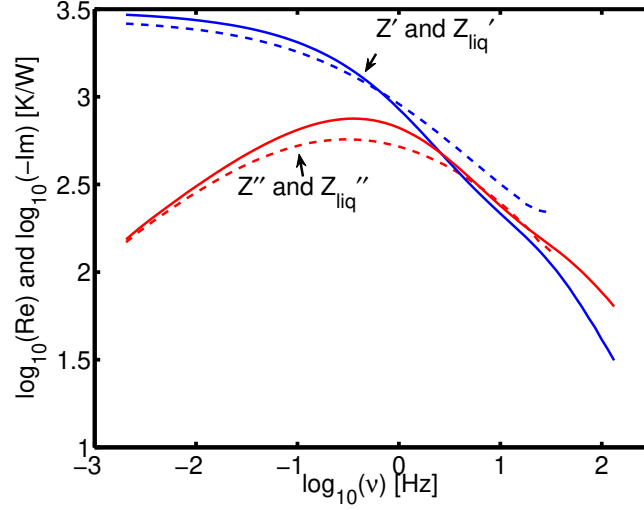


FIG. 9: Comparison of the raw measured thermal impedance, Z , and final liquid thermal impedance, Z_{liq} , corrected for the influence of the thermistor encapsulation. Data are taken at room temperature ($T = 295.6\text{K}$), and are equivalent to the data shown on Fig. 4. The liquid thermal impedance is truncated at high frequencies ($\nu > 10^{1.5}\text{Hz}$) as the bead becomes dominant at higher frequencies, leading to unphysical behavior of the calculated liquid impedance. **Full lines:** Raw thermal impedance Z . **Dashed lines:** Liquid thermal impedance Z_{liq} .

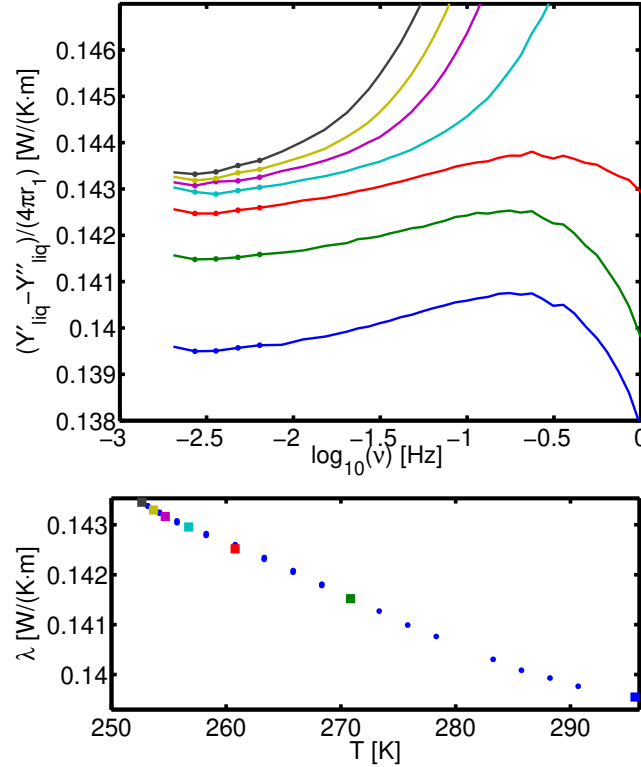


FIG. 10: Thermal conductivity of the liquid. **Top:** $\frac{Y'_{\text{liq}} - Y''_{\text{liq}}}{4\pi r_1}$ as function of frequency, plotted for a selection of temperatures (same temperatures as on Fig. 11). According to Eq. 48 the thermal conductivity is the low frequency limit of this quantity. The points on the lines indicate the data points used for defining the low frequency limit (taken as an average over these points). **Bottom:** Thermal conductivity of the liquid defined from the average over the low frequency limit of $\frac{Y'_{\text{liq}} - Y''_{\text{liq}}}{4\pi r_1}$. Squares corresponds to the curves shown on the upper figure.

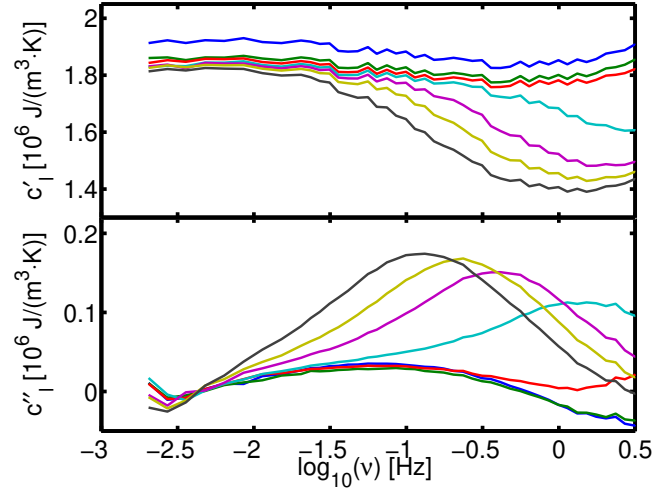


FIG. 11: Real and imaginary part of the longitudinal specific heat of the liquid, c_l , at a number of the investigated temperatures. The frequency axis is truncated at 0.5Hz as the signal above this frequency is dominated by the inner-structure of the thermistor. Temperatures are 295.6K, 270.8K, 260.8K, 256.7K, 254.7K, 253.7K, and 252.7K.

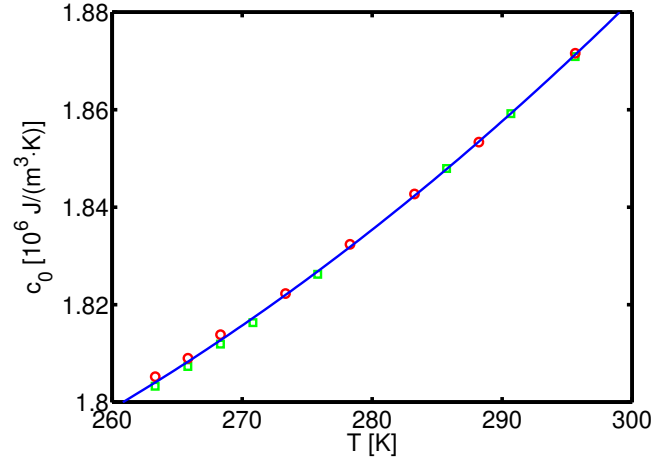


FIG. 12: DC specific heat, c_0 , of the liquid for temperatures above the liquid glass transition temperature range. The specific heat is found as the average over the real part of c_l in the frequency range 10^{-2} Hz–1Hz. c_0 corresponds to the DC value of c_p as can be seen from Eq. (3) and Eq. (4). **Open squares:** Data taken going down in temperature. **Open circles:** Data taken going up in temperature. **Line:** Best fit to a second order polynomial (the choice is purely phenomenological) $c_0(T[\text{K}]) = 13.06T^2 - 5.22 \cdot 10^3T + 2.27 \cdot 10^6$ [J/(m³ · K)].

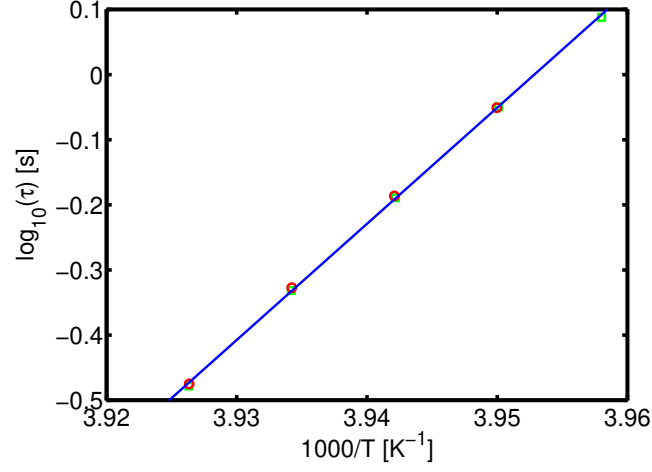


FIG. 13: Characteristic relaxation time, τ , for the longitudinal specific heat, $c_l(\omega)$. The time is found from a fit to a Cole-Cole function and corresponds to $\tau = 1/(2\pi\nu_{lp})$, where ν_{lp} is the frequency of maximum loss. **Open squares:** Data taken going down in temperature. **Open circles:** Data taken going up in temperature. **Line:** Best fit to a straight line $\log_{10}(\tau(T[K])) = 17.83 \frac{1000}{T} - 70.45$ [s]

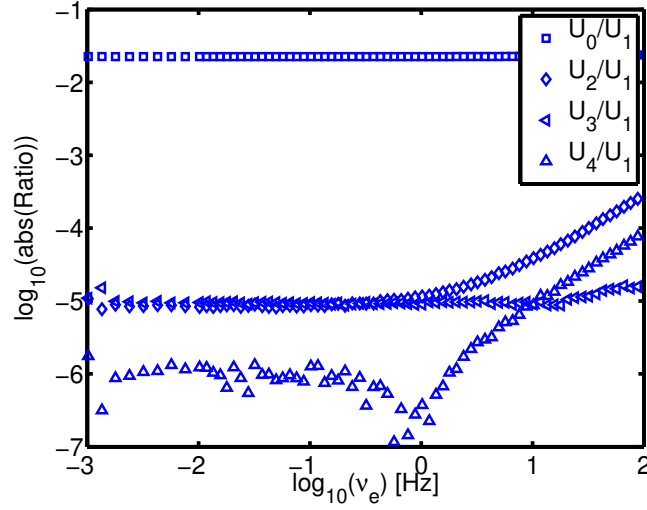


FIG. 14: Relative magnitude of the components of input voltage U to the dominant U_1 component. $\langle |U_1| \rangle = 3.927\text{V}$. See also table III.

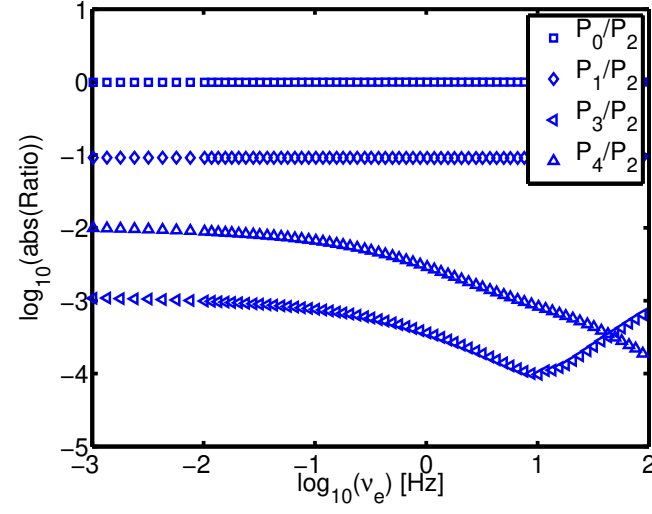


FIG. 15: Magnitude of the components of the power to the dominant P_2 component. $\langle |U_1| \rangle = 3.927\text{V}$, $T_{\text{cryo}} = 249.5\text{K}$. See also table IV.